

The Salt Spray Environments for Mechanical Degradation of welded SS304 Stainless Steels

Tung-Yung Yung, Ming-Feng Chiang, Ting-Yu Liu

Abstract— Stainless steel 304 (SS304) spent fuel canisters and casks could be attacked by saline environment during the dry storage period. The welding zone is the most sensitive position to initiate cracks. For concerns on long-term storage safety, the degradation behavior for welding zone should be monitored. Slow strain rate tensile tests (SSRT) were conducted to determine the tensile strength and notched tensile strength (NTS) of welded SS304 in 5 wt% saline spray environments at 85 °C. Both YS and UTS of the weldment were no significantly variation in either saline spray environments. A strain decrease was observed, however. Moreover, a specimen with notch could exacerbate corrosion degradation and aggravate the hydrogen embrittlement of SS304 in the saline environment. Although the welding and cold-rolled SS304 were exhibited similar mechanical features in saline environments, the lower ductile weldment could be more dangerous for the spent nuclear fuel canisters and casks. Local accumulation to higher NaCl concentration is a crucial factor affecting the susceptibility of degradation of SS304 installations in the real storage environment.

Index Terms— stainless steel 304, slow strain rate test, hydrogen embrittlement, dry storage.

I. INTRODUCTION

As a common practice, nuclear power plants have tentatively stored spent fuel in a spent fuel pool. Since the Fukushima Daiichi nuclear disaster, the interim method of fuel dry storage has become a major option which is easily administrated with lower risk and with more convenience in transportation outside of plants [1]. The SS304 dry storage canisters are used to keep the spent fuel in integrity and prevent the fission products from leakage. The vessel consists of a metal shell with one to three metal lids sealed by multi-pass welds or by bolts with metal seals. The temperature of the canister with spent fuel is estimated to be at around 200°C(473K) of the inner surface and at about 80 to 90°C(353 to 363K) of the outer surface during the first few years after cask loading, and it would maintain below 80°C (353K) in remaining storage period. There has been no severe radiation release affecting the public, no radioactive contamination, and no suspected attempts to sabotage the storage canister over the last 20 years [2]. However, the interim storage has not yet been proven fully safe for storage longer than 20 years and the existing dry storage systems worldwide will still be in

Manuscript received Feb. 20, 2014.

Tung-Yung Yung, Devison of Nuclear Fuels and Materials, Institute of Nuclear Energy Research, Lontang Township, Taoyuan, 32501, Taiwan, R.O.C.

Ming-Feng Chiang, Devison of Nuclear Fuels and Materials, Institute of Nuclear Energy Research, Lontang Township, Taoyuan, 32501, Taiwan, R.O.C.

Ting-Yu Liu, Department of Materials Engineering, Ming Chi University of Technology, New Taipei City 24301, Taiwan, R.O.C.

need to extend the certain service lives. For these reasons, researches of cask materials especially on degradation behaviors, thermal fatigue and environmental corrosion would be very demanding subjects in next few years. Saline corrosion will be a concern for metal components exposed to humid environments along the seacoast, as many interim storage systems were located near the seashore. Severe corrosion of stainless steel canisters with the chloride ion and water vapor in the atmosphere would pose a grave threat to the operational safety and reliability of interim dry storage systems. For these systems, the welding areas of the stainless steel canisters and casks are considered as an initial location towards the stress corrosion cracking (SCC), attributed to the welding residual stress and sensitization [3].

Austenitic stainless steels are extensively used in the nuclear industry because of their good anti-rust performance in corrosive environments, in addition to excellent ductility, formability, toughness, and weldability. However, the mechanical property and corrosion resistance of AISI 304 austenitic stainless steels (SS304) changeable with sensitization have been reported [4-8], which could be accounted by microstructure evolution with welding thermal cycles. Chromium-rich carbides are formed within the temperature range of 500–750 °C, with continuation to grow at much lower temperatures, however. Thermal sensitization is by heat treatment and welding process whereas low temperature sensitization occurs below the chromium-rich carbide precipitation temperature during long-time storage [3]. A wide number of reports have shown that sensitization is a significantly factor of grain boundary chromium depletion and it seems to be detrimental to inter grain stress corrosion crack (IGSCC) under chloride condition [3, 5, 6, 9-11]. The cask surfaces are the areas of chloride deposition with higher saline concentration, which increases the pitting sensitivity and assists the crack propagation of austenitic stainless steel [12-14]. Although the NaCl concentration is usually lower than 5ppm in the moist atmosphere near the seashore. Some localized spots, like the lid or bottom edge on a canister surface, are with a higher saline concentration and hence with condensed NaCl deposits. These salt deposited areas usually have a large number of welding structures and always degrade quickly. The creviced bend beam and compact tension tests on SS304 and SS316 had been done in solutions of high chloride concentrations [15-18], but the degradation behaviors of the canister materials in lower concentration of saline atmosphere have not been well studied yet, especially with the welded metal. In order to understand the reliability of the storage canisters in the saline atmosphere, the corrosion resistance and mechanical properties of SS304 with welding structure should be evaluated, with local accumulation of NaCl concentration a crucial factor in mind.

In this work, the fracture behavior and chloride corrosion durability of welding SS304 in 5 wt% saline spray

environments were investigated and compared with the cold work specimens. Since the slow strain rate technique provides useful information on SCC susceptibility of materials in any corrosive environment in a relatively short time span [16], all of the mechanical evaluation was studied with a SSRT. The notch tensile specimen tests were also conducted in this work to elucidate the notch fracture behavior of stainless steel in the saline atmosphere. The fracture surface and cross-sectional microstructures were examined for understanding the mechanism of the saline environment SSRT.

II. EXPERIMENTAL SECTION

The base materials were used in the welding type 304 forged stainless steel plates with 17 mm thickness. The welding wire used is 308L bare wire with a 0.9 mm diameter. The chemical compositions of the base and weld metals are summarized in Table 1. The weld design and procedure are including both cold-wire and hot-wire feeding processes. The welding was performed using an automatic gas-tungsten arc welding (GTAW) machine at the welding speed of about 5.1 cm/min (2 in/min) for cold-wire and 5.1 cm/min (2 in/min) for hot-wire. The heat input rate is about 20 KJ/cm (50 kJ/in) for the former and 20 KJ/cm (50 kJ/in) for the latter.

The SSRT specimens were tested with a slow strain rate tension testing machine equipped with a salt spray system at a strain rate of 1×10^{-6} /s at 85°C (358K), with the loading direction for the SSRT specimen parallel to the rolling direction. The test atmosphere was kept with a spray of 5 wt% NaCl solution until the specimen failed. Three sets of test data were averaged to give a mean value for each test condition. Summarized in Tables 2 is the mean measurements obtained for non-notched SSRT and notched SSRT specimens, respectively. The fracture features of the specimens were tested in varying environments with Hitachi S4800 scanning electron microscopy (SEM). And the cross-sectional of the notched and non-notched SSRT specimens in 5% saline environment were examined with the Oxford electron back scattering diffraction (EBSD) for identity of the crystalline phases.

III. RESULTS AND DISCUSSION

The difference of 304 and 308L stainless steel materials is on the contents of Cr and Ni such that 308L stainless steel has greater amounts of Cr and Ni than 304. After welding, the condensation structures of the 308L weldment are α -ferrite, γ -ferrite and δ -ferrite. The δ -ferrite is present only after the welding process and the δ -ferrite is absent before the welding. Accordingly, the δ -ferrite in the weldment of the SSRT specimens would be as the key factor of the SCC. The amounts of martensite in the cold-rolled specimens of different reductions were measured by a ferrite scope. The martensite content near the specimen surface increased as the cold roll reduction increased. The quantity of ϵ -martensite for the specimen of 30% cold roll reduction was apparently more than that for the as-received one. The ferrite numbers were also increased with the cold-rolled percentage [19-20]. In this study, we eliminated the cold-rolled effects.

The fractural images were shown in Figure 1, that the smooth specimens and notched specimens were different in the ductility. The smooth specimens were more ductile and more elongated than the originals. The SSRT fracture

surfaces of smooth and notched specimens in ambient environment were shown in Figure 2 (a) and Figure 3 (a) that the edges were obviously extended and the inner morphology of the edge was dimple structures which were typical SSRT results. In the 5% saline environment, the edge of the smooth sample was shown to produce a different morphology from that of the previous specimen. The saline reaction zone or the corrosion structures were clearly located as shown in Figure 3(b) and Figure 3(d). The dimple-liked structure was not found from the edge of the surface. Yet, the inner spaces exhibited obviously the dimple-liked structures as the SSRT results. The EDS result showed seemingly the saline reaction zone with presence of chloride. The saline corrosion with slow strain rate was found leading to that the morphology was seen with sheet-on-sheet or layer-on-layer the strain rate and the secondary cracks, as shown in Figure 3(b) and Figure 3(d). The central areas of all specimens under ambient and 5% saline environments revealed the dimple-liked morphologies with different pole sizes and shapes. The smooth specimens under two experimental environments were almost the same in shape but the pole sizes were larger in the 5% salt spray experiment. The notched samples showed the valley and ridge like shapes. And the pole sizes were more widely distributed than the smooth ones, shown in Figure 4 and Figure 5.

Our previous study of the 304 stainless steel plates with cold-roll to various degrees of reduction had shown that equiaxial austenite grains with annealed twins were found in the as-received (AR) specimen [21]. The cold-rolled specimens (CR) showed needle and band structures. The needle grains increased with increasing cold roll degree of reduction. Furthermore, the microstructure of the cold rolled specimen at 30% reduction (CR30) exhibited noticeable band structure. The amounts of martensite in the cold-rolled specimens of different reductions were measured by a ferrite scope. The martensite content near the specimen surface increased as the cold roll degree of reduction increased. The quantity of ϵ -martensite for the cold rolled specimen at 30% reduction was apparently more than that of the as-received one. The ferrite numbers increase with the increase of cold-rolled percentage. In this study, we eliminated the cold-rolled effects.

Figure 6 shows the EBSD results for a welded 304 specimen in 5% saline SSRT. There were the presence of cracks, δ -ferrite, and γ -ferrite (austenite cubic phase). It was a sound evidence of mechanical degradation of the SSRT in saline environment such that cracks or failures occurred by the δ -ferrite/ γ -ferrite phase boundaries. Figures 7(c) and 7(d) revealed that the δ -ferrite phase could be located between two different facets of γ -ferrite phase. Furthermore, the cracks with residual δ -ferrite phases were found in Figure 7. The notched welded 304 sample in saline SSRT was also found with the residual δ -ferrite phases that were shown in Figure 8. The fractural cross-section SEM image was compared with the EBSD IQ plus colored δ -ferrite phase image. The fractures with residual δ -ferrite phases and the cracks were induced following the δ -ferrite phases as shown in Figure 9(b). The difference of 304 and 308L stainless steel is in the contents of Cr and Ni, 308L being with greater amounts of Cr and Ni than 304. After welding, the condensation structures of the 308L weldment are α -ferrite, γ -ferrite and δ -ferrite, etc. The δ -ferrite phases were present after the welding process, whereas the δ -ferrite phases were absent before the welding.

Therefore, the δ -ferrite in the weldment of the SSRT specimens would be the key failure factor of the SCC.

IV. CONCLUSION

The fractures and cracks of SSRT samples in 5wt% NaCl atmosphere environment with 1×10^{-6} cm/s stain rate at 85°C were examined using SEM and EBSD for confirmation that the failure factor was the δ -ferrite phases. The non-notched specimen showed that the residual δ -ferrite phases were at the edge of cracks, while the notched samples revealed the residual δ -ferrite phases were at the fractural surface. After welding processing, the δ -ferrite phases were increased. In our experimental environments, δ -ferrite would be weakened the mechanical strength as the SSRT results, both in notch and non-notch specimens. The δ -ferrite would be the origin of mechanical degradation initiation and propagation.

ACKNOWLEDGMENT

The authors are thanks to the financial support from Institute of Nuclear Energy Research.

REFERENCES

- [1] K. Shirai, "Status of Spent Fuel Management in Japan and Key Issues on R&D Activities", US Nuclear Used Fuel Strategy Conference, Charlotte, USA, 28-29 Nov., 2012
- [2] T. Saegusa, K. Shirai, T. Arai, J. Tani, H. Tankeda, M. Wataru, A. Sasahara and P. L. Winston, Nucl Eng Tech., 42, (2010), 237-248
- [3] D. Itzhak and D. Eliezer, Corros. Sci., 23, (1983), 1285-1291
- [4] H. T. Lee, Y. D. Lin, T. Y. Kuo and S. L. Jeng, Mater. Trans., 48 (2007), 1538-1547
- [5] R. Nishimura and Y. Maeda, Corros. Sci., 46 (2004) 769-785
- [6] R. Nishimura and O. M. Alyousif, Corros. Sci., 51 (2009) 1894-1900.
- [7] Garcia, F. Martin, P. De Tiedra, J. A. Heredero and M. L. Aparicio, Corros. Sci., 43 (2001) 1519-1539
- [8] C. Garcia, F. Martin, P. De Tiedra, J. A. Heredero and M. L. Aparicio, Corros. Sci., 43 (2001) 1519-1539
- [9] C. L. Lai, L. W. Tsay, W. Kai and C. Chen, Corros. Sci., 51 (2009) 380-386
- [10] C. García, F. Martín, P. De Tiedra, J. A. Heredero and M. L. Aparicio, Corros. Sci., 43 (2001) 1519-1539
- [11] M. A. Arafin and J. A. Szpunar, Corros. Sci., 51 (2009) 119-128
- [12] M. O. Speidel, Metal. Trans. A 12A (1981): p.779
- [13] P. M. Singh, O. Ige and J. Mahmood, Corrosion 59 (2003): p.348
- [14] C. Garcia, F. Martin, P. De Tiedra, J. A. Heredero and M. L. Aparicio, Corros. Sci. 43 (2001): p.1519
- [15] S.V. Phadnis, A. K. Sapati, K. P. Muthe, J. C. Vyas and R. I. Sundaresan, Corros. Sci., 45 (2003) 2467-2483
- [16] A. K. Singh, V. Chaudhary and A. Sharma, Portugaliae Electrochimica Acta, 30, (2012) 99-109
- [17] O. M. Alyousif and R. Nishimura, Corros. Sci., 48 (2006) 4283-4293
- [18] O. M. Alyousif and R. Nishimura, Corros. Sci., 49 (2007) 3040-3051
- [19] J. Kuniya, I. Masaoka and R. Sasaki, Corros. Sci. 44 (1988) 21-28
- [20] S. Ghosh and V. Kain, Mat. Sci. Eng., A527 (2010) 679-683
- [21] M. J. Chiang, H. L. Hsu and M. J. Yang, J. Nuclear Mater., 441 (2011) 83-89



Tung-Yuan Yung, National Central University, Physics PhD candidate 2012, Associate Researcher at Industrial Technology Research Institute 2002-2006, Assistant Engineer at Institute of Nuclear Energy Research 2006-present. His works on the materials for solid oxide fuel cells, PEM fuel cells and other energy-related materials.



Ming-Feng Chiang, National Taiwan University, MSE, PhD 2010, Associate Engineer at Institute of Nuclear Energy Research 2010-2012, Engineer at China Steels Co. 2012-present. His works are on the materials properties after welding.



Ting-Yu Liu, National Chiao Tung University, MSE PhD 2008, Assistant Professor, Polymer Institute at National Taiwan University 2010-2013, Assistant Professor, Materials Engineering at Ming Chi University of Technology 2013-present. His current research interest includes nano- and bio-interface related materials.

Table 1. The chemical compositions of the materials

	C	Cr	Ni	Mn	Mo	Co	Si	P	S	Cu	Fe
304	0.08	18.1	8.81	1.56	0.28	0.1	0.50	0.03	0.0004	0.48	Bal.
308L	0.02	22.00	14.50	1.70	2.70	--	0.50	0.015	0.005	--	Bal.

Table 2. The results of SSRT in different experimental environments

	YS (MPa)	UTS (MPa)
308L Ambient (Non-Notched)	470.4	561.1
Ambient (Non-Notched)	398.7	553.4
5% Saline (Non-Notched)	374.1	550.7

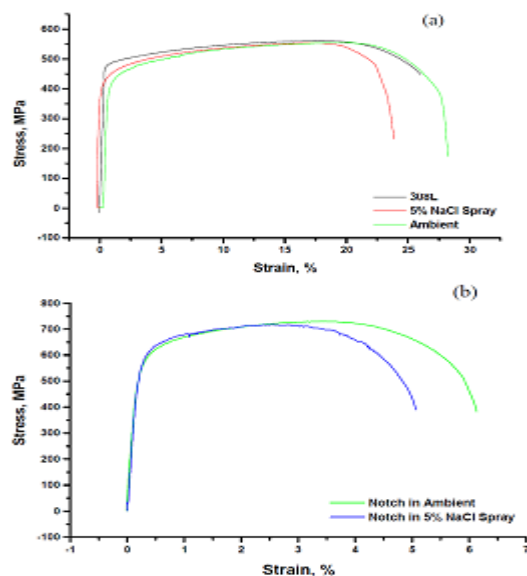


Figure 1. The SRRT results in ambient and 5 wt% saline environments at 85°C (a) specimen without notch (b) notch specimens



Figure 2. The fractural samples of the notched in ambient, the notched in 5% salt spray, the non-notched in ambient and the non-notched in 5% salt spray from left to right, respectively.

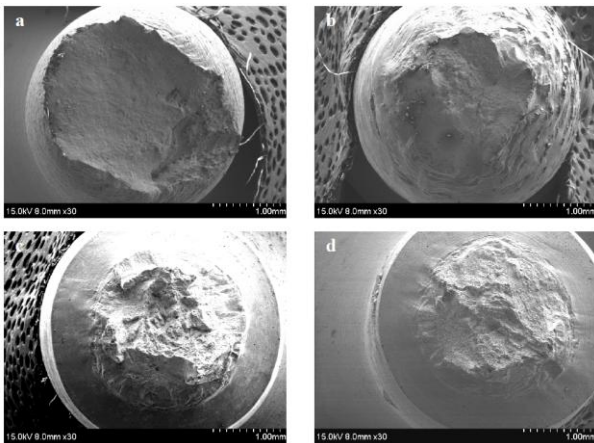


Figure 3. The fractural surfaces of the SSRT (a) non-notched specimen in ambient (b) non-notched sample in 5% saline environment (c) notched sample in ambient (d) notched sample in 5% saline environment.

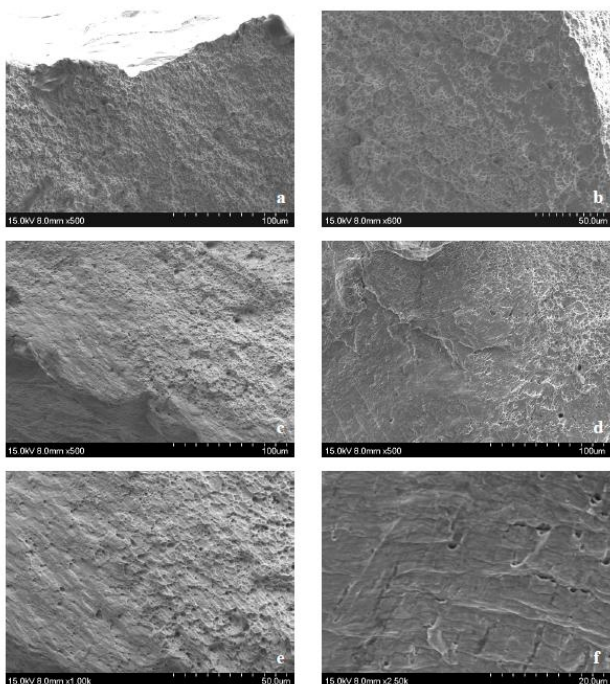


Figure 4. The edges of the SSRT specimens (a) non-notched in ambient (b) non-notched in saline atmosphere (c) notched in ambient (d) notched in saline atmosphere (e) notched in ambient at the 1000X (f) notched in saline atmosphere at 2500X.

Figure 5. The edge of the fractural surface by variant magnificient SEM microscopy images (a) SSRT sample in ambient with 500X (b) SSRT notch sample in 5% saline environment with 250X (c) SSRT notch sample in 5% saline environment ambient with 500X (d) SSRT sample in 5% saline environment with 2000X.

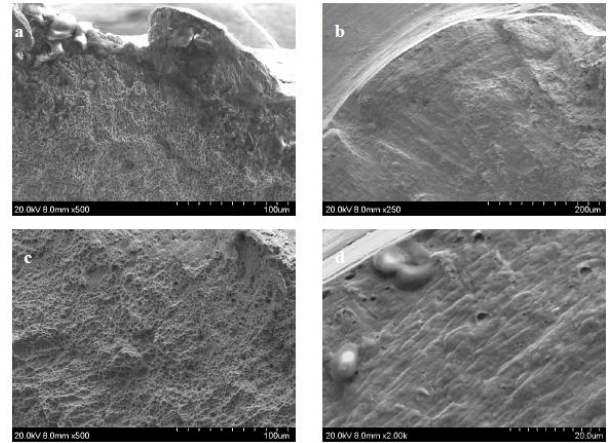


Figure 6. The center of the fractural surface by SEM microscopy images (a) SSRT sample in ambient (b) SSRT sample in 5% saline environment (c) SSRT notched sample in ambient (d) SSRT sample in 5% saline environment.

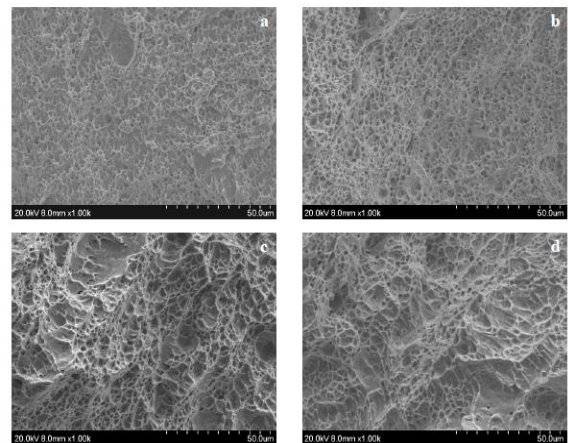


Figure 7. The cracks EBSD of the SSRT sample without notched with EBSD results. (a) the EBSD pattern (b) the pink color for the δ-ferrite phase and the yellow for austenite cubic phase (c) and (d) the color distribution of austenite cubic phase with [001], [101] and [111] facets.

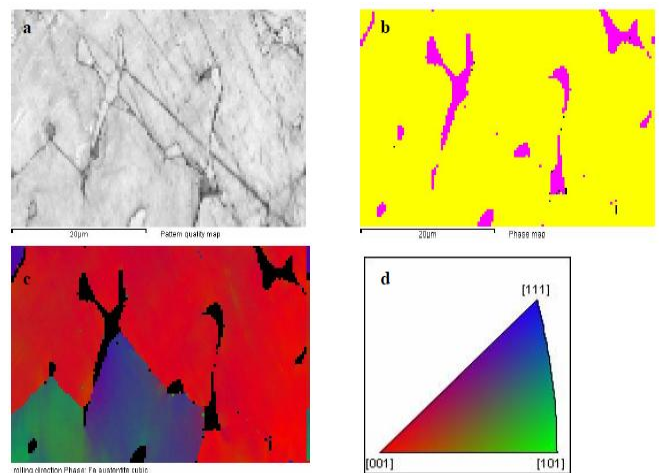


Figure 7. The cracks EBSD of the SSRT sample without notched with EBSD results. (a) the EBSD pattern (b) the pink color for the δ-ferrite phase and the yellow for austenite cubic phase (c) and (d) the color distribution of austenite cubic phase with [001], [101] and [111] facets.

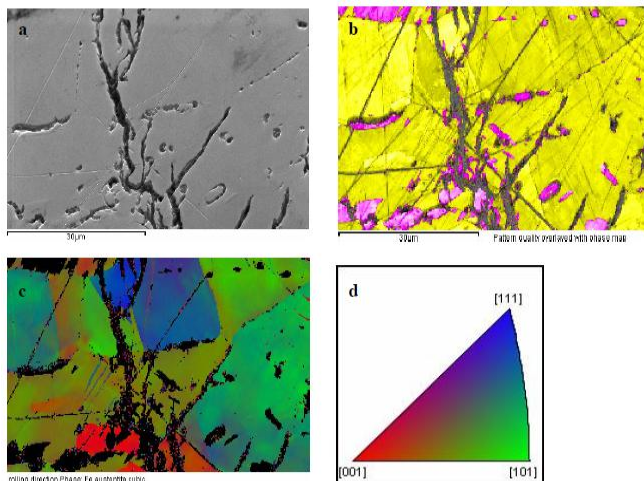


Figure 8. The EBSD cracks features of the SRRT sample without notched (a) the EBSD pattern (b) the pink color for the δ -ferrite phase and the yellow for austenite cubic phase (c) and (d) the color distribution of austenite cubic phase with [001], [101] and [111] facets.

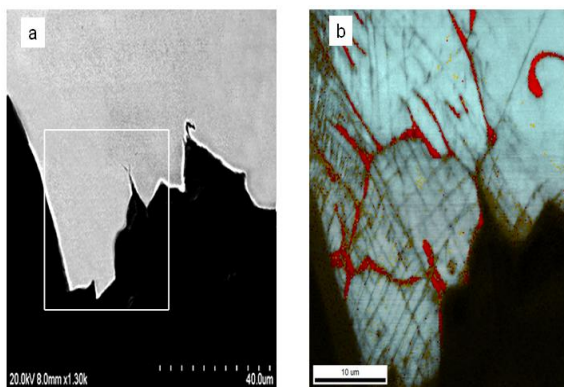


Figure 9. Figure 10. The cracks features of the SRRT sample with notched. (a) the SEM of notched edge of the fracture (b) the EBSD result for notched edge (the white frame area from (a)), the red color is for δ -ferrite phase.